Analysis of Transonic Cascade Flow Using Conformal Mapping and Relaxation Techniques

David C. Ives* and John F. Liutermoza†
Pratt & Whitney Aircraft, East Hartford, Conn.

Conformal mapping and relaxation techniques are applied to the computation of supercritical cascade flow. A conformal transformation enabling the mapping of cascades found in engines and a conformal transformation producing an improved finite-difference grid are introduced. A variant of the standard line-relaxation implementation, called "dynamic sweeping," has been found to enhance the stability of the transonic relaxation process. Calculations are presented for the test cases of Gostelow and Korn to demonstrate the accuracy that can be achieved with modest computation times.

Introduction

THE transonic flow occurring in turbines and advanced compressors requires an accurate analysis technique. A two-dimensional calculation method has been developed which achieves high accuracy in conjunction with modest computation times through the use of conformal mapping and relaxation techniques.

A conformal mapping is used to map the region exterior to a cascade of identical blades onto a rectangular computational domain. This mapping, for a uniform mesh in the computational domain, produces a grid that is automatically dense near the nose and trailing edge of the blades, where a fine grid is necessary to resolve the details of large gradients in flow properties. The grid is relatively uniform across the channel, where (except for shock waves) there are only moderate flow gradients. The regions far upstream and far downstream from the cascade blades, where flow gradients are small, are each collapsed into a point in the computational plane so that a desirable sparse grid is obtained in the cascade plane far from the blades. The cascade periodicity condition is reduced by the mapping to a simple continuity condition. The blade surface boundary condition of zero normal velocity is easily satisfied to second-order accuracy, as the blade surface becomes a coordinate line in the mapped computational plane. To achieve a conformal mapping having all of these qualities and which would work for blade geometries found in engines required two basic advances over methods reported in the literature.[1-5]

The full transonic potential flow equation is solved using the finite-difference procedure of Jameson,[6] wherein central differences are used in subsonic regions and a rotated backward difference scheme is used in supersonic regions to insure the correct domain of dependence. Line relaxation is used to solve the finite-difference equations, and the damping terms of Jameson have not been necessary.

The line of relaxation must be swept downstream in supersonic regions for stable calculations. Unlike the isolated airfoil case, the a priori estimation of the location of supersonic regions is difficult for a cascade because of the large flow incidence variations encountered during typical engine operation. The placement of the line sweep start and finish limits depends on these supersonic region locations. A modification of the standard line-relaxation implementation, called "dynamic sweeping," was developed to position the sweep sequence for a relaxation cycle according to the nose and tail stagnation points obtained from the previous relaxation cycle. The modified method is stable and convergent for the cascade case, whereas the standard method with an a priori fixed sweeping sequence often diverged. This modification, along with extrapolated relaxation,[7] has resulted in a stable and rapid transonic flow calculation process.

Presented as Paper 76-370 at the AIAA 9th Fluid and Plasma Dynamics Conference, San Diego, Calif., July 14-16, 1976; submitted Aug. 6, 1976; revision received Feb. 22, 1977.

Index categories: Transonic Flow; Computational Methods; Rotating Machinery.

*Associate Research Scientist. Member AIAA.

†Senior Scientific Programmer/Analyst.

Conformal Mapping of a Cascase of Blades

This section presents the sequence of conformal transformations used to map the region exterior to the cascade of blades onto a rectangular region suitable for finite-difference computations. The first transformation of this sequence conformally maps the region exterior to the cascade of blades onto the region interior to a near circle. This new transformation is given by

$$c\frac{\omega-a}{\omega-b}=\left\{\frac{\sin\left[\frac{\pi(Z-ZT)}{H+iG}\right]}{\sin\left[\frac{\pi(Z-ZN)}{H+iG}\right]}\right\}^{1/\kappa} \tag{1}$$

where, as illustrated in Fig. 1, we have

Z = $x+iy$ = cascade plane complex coordinate
ω = near-circle plane complex coordinate
κ = $2-\tau/\pi$
τ = trailing-edge included angle
$H+iG$ = repeat vector in cascade plane

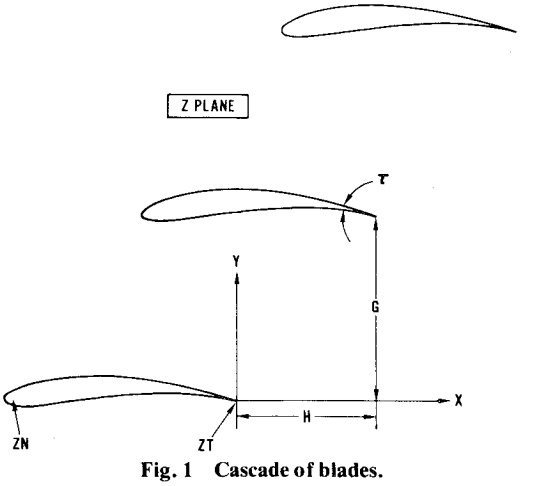

Fig. 1 Cascade of blades.

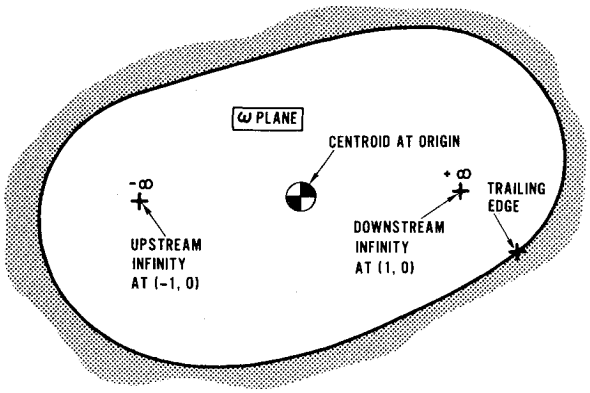

Fig. 2 Near circle.

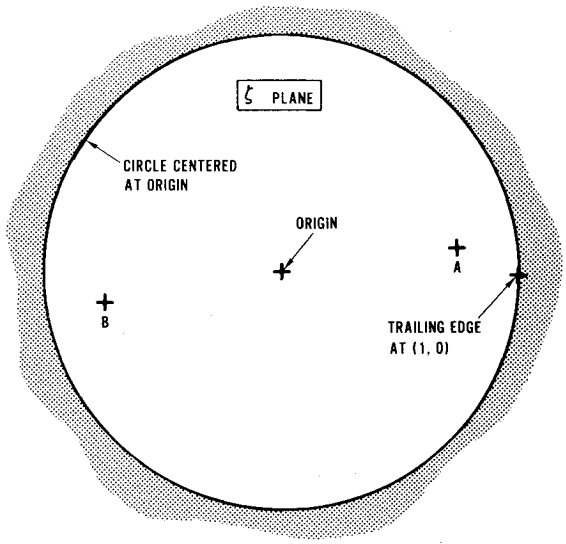

Fig. 3 Circle in ζ plane.

ZN = Z coordinate midway between the nose of a blade and its center of curvature

ZT = Z coordinate midway between the tail of a blade and its center of curvature‡

The three complex constants a, b, and c are chosen, as illustrated in Fig. 2, to satisfy the three complex conditions that 1) for Z=upstream infinity, $\omega=-1$; 2) for Z =downstream infinity, $\omega=+1$; and 3) the centroid of the ω plane near-circle shall be at $\omega=0$. The centroid in the ω plane can be defined as the centroid of the figure obtained by connecting all adjacent points by straight lines. A Newton-Raphson iteration procedure is used to determine the constants a, b, and c satisfying these three conditions by a completely automatic computerized procedure.

The conformal transformation given by Eq. (1) is regular at all finite points in the Z plane distinct from ZN and ZT and the periodic repetitions of ZN and ZT. This transformation also gives equal emphasis to the nose and tail regions. Other cascade conformal transformations are given by Garrick,[1] Howell,[2] and Legendre.[3] For flat-plate cascades at zero stagger, Eq. (1) reduces to the Garrick transformation.

The interior of the near circle in the ω plane is mapped onto the interior of a unit circle in the ζ plane by the conformal transformation

$$\omega=\zeta\exp\left[\sum_{j=0}^{j=N}(A_j+iB_j)\zeta^j\right] \tag{2}$$

‡If the nose and/or tail is sharp, ZN and/or ZT are, respectively, set equal to the nose and/or tail coordinate of any one of the blades.

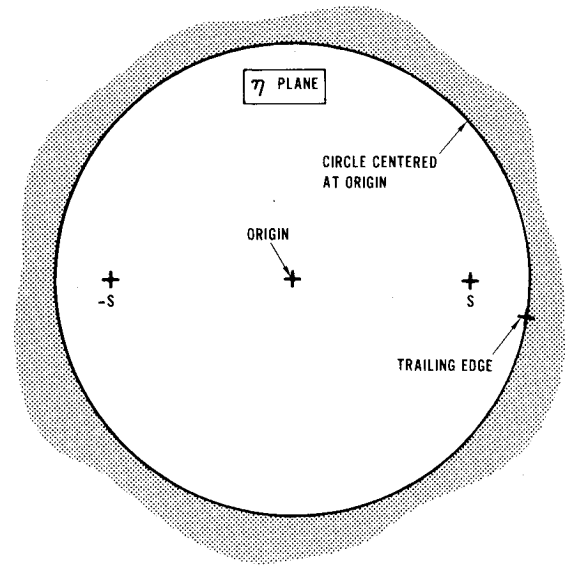

Fig. 4 Circle in η plane.

This transformation is a variant of the Theodoresen-Garrick[8] transformation for finite N, in that positive powers of ζ appropriate for an internal mapping are used in the exponent instead of the negative powers of ζ appropriate for an external mapping. Taking note of this difference, a technique nearly identical to that in Ives[9] is employed. This technique uses a periodic cubic spline to represent the near circle and fast Fourier methods to determine the coefficients A_j and B_j such that the blade trailing-edge image is mapped into $\zeta=1$. The images of downstream infinity at $\omega=1$ and upstream infinity at $\omega=-1$ are transformed into $\zeta=A$ and $\zeta=B$, as illustrated in Fig. 3.

The bilinear transformation

$$\eta=\gamma[(\zeta-\alpha)/(\zeta-\beta)] \tag{3}$$

then is used to place the images of $\zeta=A$ and $\zeta=B$ symmetrically around the origin at a distance S in the η plane, with the blade surface image becoming a unit circle centered on the origin, as illustrated in Fig. 4. The real constant S and the complex constants γ, α, and β are obtained from the equations

$$\chi=\frac{2-|A+B|^2+2|AB|^2}{|A-B|^2} \tag{4a}$$

$$S=\text{minimum of }\{\sqrt{|\chi+(\chi^2-1)^{1/2}|},\ \sqrt{|\chi-(\chi^2-1)^{1/2}|}\} \tag{4b}$$

$$\alpha=\frac{2AB+[S^2(A-B)-(A+B)]/\bar{A}}{S^2(A-B)+(A+B)-2/\bar{A}} \tag{4c}$$

$$\beta=\frac{2AB-\alpha(A+B)}{A+B-2\alpha} \tag{4d}$$

$$\gamma=S\frac{A-\beta}{A-\alpha} \tag{4e}$$

where a horizontal bar above a quantity denotes a complex conjugate, and vertical bars enclosing a quantity denote a magnitude.

The region interior to the unit circle in the η plane is mapped onto a rectangular computational plane by the conformal transformation

$$\eta=S\ \text{sn}\ [(2\kappa i/\pi)\xi+\kappa] \tag{5}$$

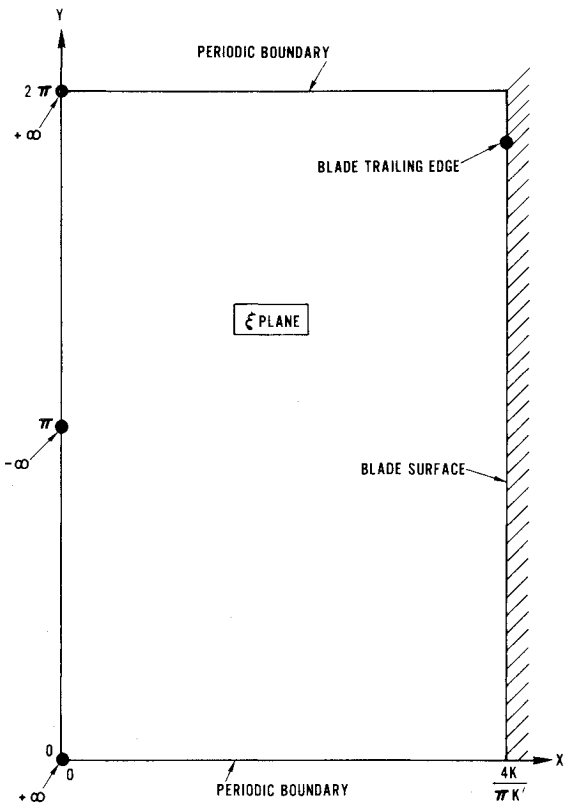

Fig. 5 Computational plane.

where

$\xi = X + iY$ = computational plane complex coordinate

$$K = \int_{\theta=0}^{\theta=\pi/2} \frac{d\theta}{\sqrt{1 - S^4 \sin^2\theta}}$$

sn = Jacobian elliptic function

The rectangular computational region, as illustrated in Fig. 5, is bounded by the lines $X=0$, $X=4\kappa/\pi\kappa'$, $Y=0$, and $Y=2\pi$, where

$$\kappa' = \int_{\theta=0}^{\theta=\pi/2} \frac{d\theta}{\sqrt{1 - (1-S^4)\sin^2\theta}}$$

The lines $Y=0$ and $Y=2\pi$ are periodic boundaries, the line $X=4\kappa/\pi\kappa'$ is the blade surface, and points along the line $X=0$ at equal distances from $Y=\pi$ have the same image point in the η plane. The image of upstream infinity is mapped into $X=0$, $Y=\pi$, whereas the image of downstream infinity is mapped into $X=0$, $Y=0$ and $X=0$, $Y=2\pi$. The slit from $\eta=-S$ to $\eta=S$ is mapped into the line $X=0$.

The image of a uniform rectangular computational grid in the ξ plane, transformed back to the cascade plane, is presented in Fig. 6. This grid displays automatic refinement near the nose and tail, a reasonably uniform mesh between blades, and a sparse mesh far from the blades, as desired for efficient numerical calculations. If we instead had created a polar coordinate grid in the η plane, as in Frith,[5] we would have obtained the grid§ of Fig. 7. This latter grid system entails special handling for the potential equation at the point where all of the radial lines meet. The mapping given by Eq. (5) avoids this difficulty and furthermore produces a grid system that does not waste grid points by over-resolving a region of the flowfield in which the flow is not varying

§This grid example does not contain the radial stretching used in Frith.

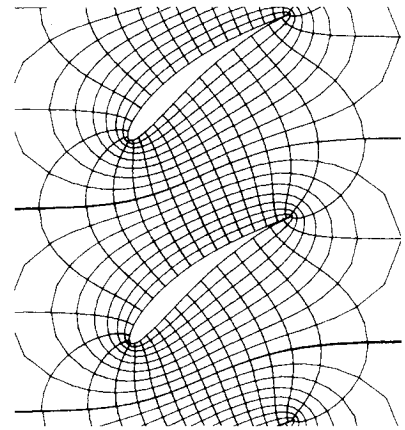

Fig. 6 Image of uniform grid in computational plane transferred back to physical plane.

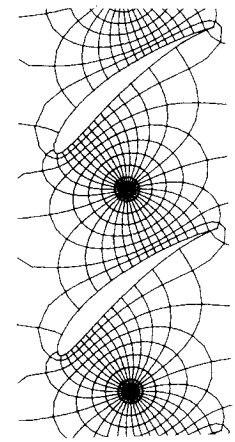

Fig. 7 Grid system using method of Frith.

rapidly. Our grid system also is more closely aligned with the flow, an important consideration for transonic relaxation calculations.

Potential Flow Equation

The equation for inviscid two-dimensional potential flow may be written in vector form as

$$\nabla^2\phi = -\nabla\phi \cdot \nabla \ell n\, \rho \tag{6}$$

where

$\nabla = \left(\hat{i}\frac{\partial}{\partial x} + \hat{j}\frac{\partial}{\partial y}\right)$ = gradient operator

ϕ = velocity potential

ρ = density

This potential flow equation, expressed in terms of coordinates in the ξ plane, is¶

$$(a^2-u^2)\phi_{XX} - 2uv\phi_{XY} + (a^2-v^2)\phi_{YY} + (u^2+v^2)(uh_X + vh_Y) = 0 \tag{7}$$

where

$u = \phi_X/h$
$v = \phi_Y/h$

¶Although it is fully realized that a conservation form would be more appropriate for cases involving strong shock waves, a non-conservation form is chosen here for simplicity.

$a^2 = [(\gamma-1)/2](1-q^2)$
$q^2 = u^2+v^2$
γ = ratio of specific heats
h = $|dZ/d\xi|$ = mapping modulus

Boundary Conditions

The blade surface boundary condition

$$\phi_X(4\kappa/\pi\kappa', Y) = 0 \tag{8}$$

is satisfied using a second-order accurate central difference formula. The periodicity requirement

$$\phi(X, Y+2\pi) = \phi(X, Y) \tag{9}$$

is satisfied by simple computer logic, which shifts reference to any point on or above $Y=2\pi$ or below $Y=0$ to a corresponding point displaced in the Y direction by an integer multiple of 2π so as to lie on the computational grid. The requirement of continuity across the slit in the η plane between $\eta=-S$ and $\eta=S$ reduces to

$$\phi(0, 2\pi-Y) = \phi(0, Y) \tag{10}$$

This equation is satisfied by updating each ϕ value on the $X=0$ line as soon as its corresponding ϕ value is altered by the line-relaxation calculation. The potential ϕ is undefined to within a constant, so we set

$$\phi(0, \pi) = 0 \tag{11}$$

The Kutta condition is imposed by requiring

$$\phi_Y(4\kappa/\pi\kappa', YT) = 0 \tag{12}$$

where YT is the Y coordinate at the trailing edge image in the ξ plane. As the trailing edge is not, in general, a grid point, we satisfy Eq. (12) by using a second-order accurate difference formula involving values of ϕ at the three points on the blade grid nearest the trailing edge. If the blade trailing edge is rounded, as in a turbine cascade, then either the downstream flow angle or speed can be specified instead of Eq. (12).

The equation for global mass balance is

$$(\rho q \cos\theta)_1 = (\rho q \cos\theta)_2 \tag{13}$$

where stations 1 and 2 are at upstream and downstream infinity in the Z plane. At these stations, the flow is uniform and inclined at an angle θ with respect to the Z plane x axis.

Singularity Removal

The potential at the images of upstream and downstream infinity is that of a source and vortex. To remove this singular behavior of the potential from our finite-difference equation, we set

$$\phi = \phi^R + \phi^S \tag{14}$$

where ϕ^S is the singular potential due to appropriate sources and vortices at $\eta=S$ and $\eta=-S$. The singular potential then may be expressed as

$$\phi^S = Re\,\{(A+iB)\ln(\eta+S) + (C+iD)\ln(\eta-S)\} \tag{15}$$

The constants A and B are determined uniquely by the given upstream flow speed and inclination. The quantities C and D are obtained using a Newton-Raphson iteration such that Eqs. (12) and (13) are satisfied.** As the upstream infinity Mach number goes to zero, ϕ^S becomes the incompressible solution.

**It should be noted that mass is conserved on a global basis analytically by the choice of ϕ^S, but shock waves can result numerically in local mass creation or destruction because of our choice of a nonconservative difference scheme.

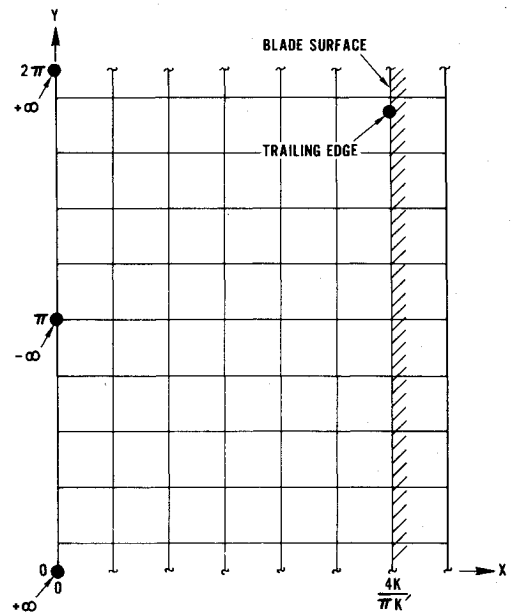

Fig. 8 Computational grid system.

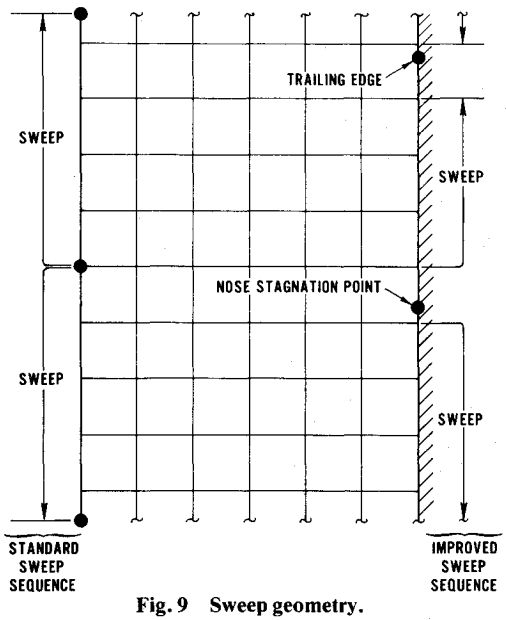

Fig. 9 Sweep geometry.

The mapping modulus h is also singular at the image points in the ξ plane corresponding to upstream and downstream infinity. To remove this singular behavior, we set

$$h = \frac{g}{\sqrt{\cosh 2X - \cos 2Y}} \tag{16}$$

Upon substitution of Eqs. (14-16) into Eq. (7), we obtain a regularized two-dimensional potential flow equation in terms of ϕ^R and g which is suitable for finite-difference solution, in that derivatives of ϕ^R and g are nonsingular.†† All derivatives of ϕ^S and $\sqrt{\cosh 2X - \cos 2Y}$ are obtained analytically. Closer examination reveals that the regularized potential equation, although nonsingular, becomes indeterminate at the images of upstream and downstream infinity. At the upstream infinity image, we simply apply Eq. (11) instead of the potential equation. To avoid the need for special handling of the regularized potential equation at the downstream infinity

††At a sharp tail or nose, g is singular, and care should be taken to form the necessary derivatives of g with difference expressions that do not include points on both sides of the singularity.

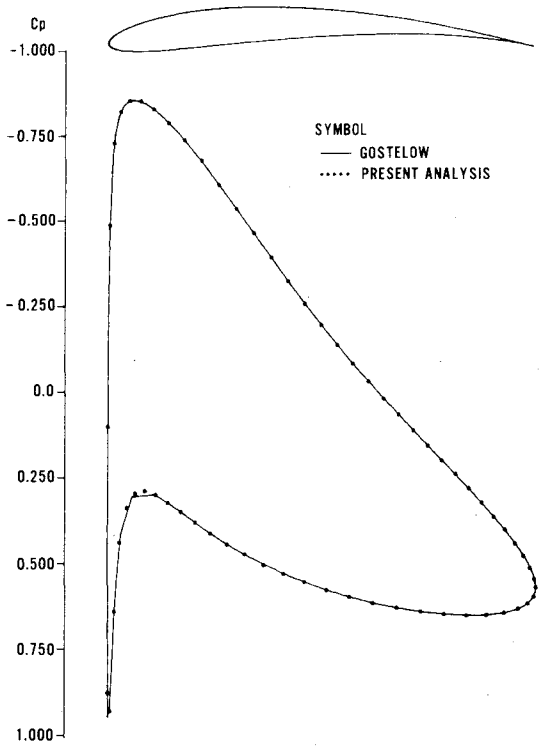

Fig. 10 Pressure coefficient for Gostelow cascade.

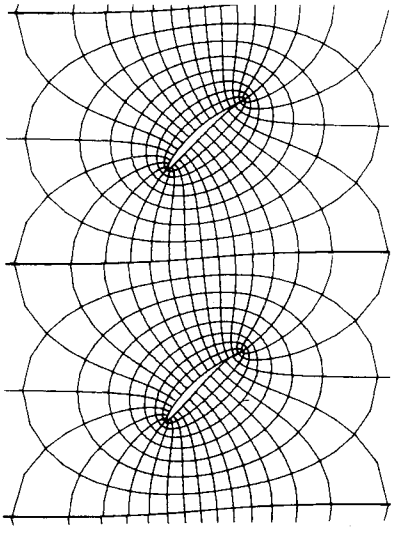

Fig. 11 Cascade plane grid image for Korn compressor cascade.

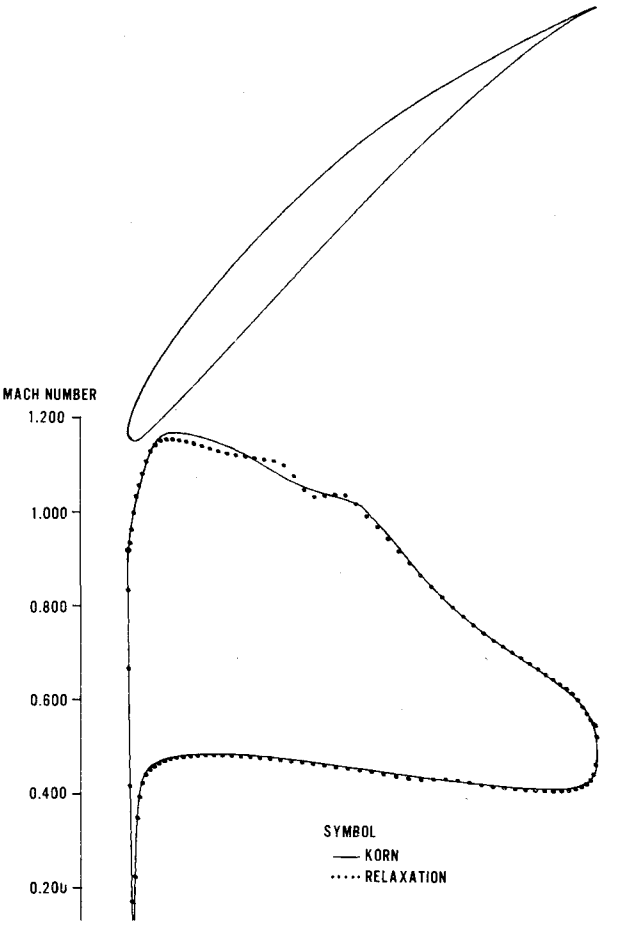

Fig. 12 Mach number plot for Korn cascade.

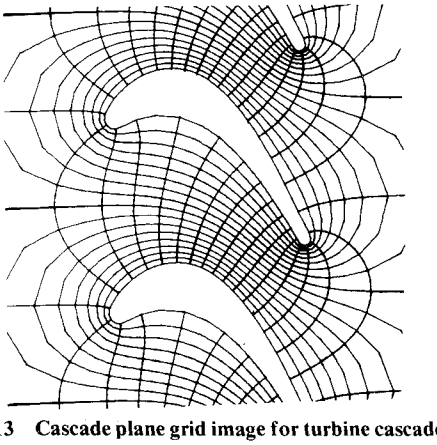

Fig. 13 Cascade plane grid image for turbine cascade.

image point, we construct a grid system such that this point is midway between grid lines, as illustrated in Fig. 8.

Difference Equations and Relaxation Solution

The regularized two-dimensional potential flow equation is reduced to finite-difference form by the procedure of Jameson,[6] wherein central differences are used in subsonic regions and a rotated backward difference scheme is used in supersonic regions to insure the correct domain of dependence. The damping terms described in Jameson are not included, as they have not proven necessary for our calculations.

To achieve iterative convergence for cascade flows, a "dynamic sweeping" modification was made to the standard-line relaxation implementation. This modification places the line sweep start and finish limits to straddle the nose and tail stagnation-point locations from the previous iteration cycle, as illustrated in Fig. 9. These (dynamic) limits change during the relaxation process and insure that the line of relaxation is swept downstream in supersonic regions to prevent non-convergent or divergent relaxation iterations. With standard fixed limits (as used in isolated airfoil calculations) the cascade calculations often diverged, whereas with dynamic sweeping the iterations converged. This dynamic sweeping iteration process is stable and convergent even for cases in which the flow through the cascade is fully choked. The technique of "extrapolated relaxation," as described in Caughey and Jameson,[7] has been used to further accelerate the convergence process.

Computed Examples

An exact test case for incompressible cascade flow has been generated by Gostelow[10] using an inverse conformal mapping method. This exact test case is the one used in Figs. 1-7 to

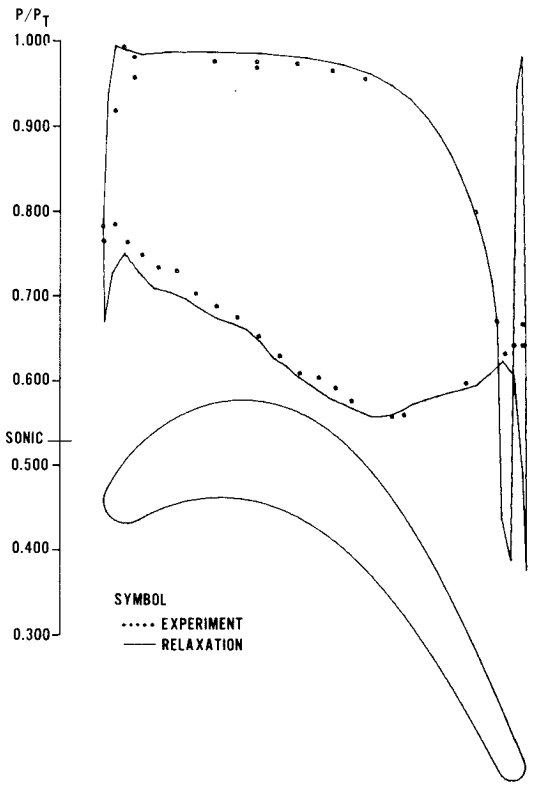

Fig. 14 Pressure distribution for turbine cascade.

illustrate the mapping sequence. The incompressible flow over this cascade was calculated using the method presented here by setting the upstream Mach number equal to 0.001. The relaxation iteration terminated after one cycle for this case, with a maximum residual less than 10^{-6}. The blade pressure coefficient obtained by using only the upstream flow inclination and blade geometry from Gostelow, and imposing a Kutta condition at the sharp trailing edge, is presented in Fig. 10. The agreement with the Gostelow calculation is essentially perfect, verifying that our mapping and singular potential are correct.

A hodograph solution for transonic flow over a compressor cascade with 10° of flow turning has been supplied by Korn.[11] The cascade and computational grid image for this case are shown in Fig. 11, while a Mach number plot is given in Fig. 12. The agreement between the present calculation and that of Korn is excellent for subsonic regions and good in the supersonic region. The grid used for this case consisted of 32×129 points and required 80 relaxation sweeps.

A final example is that of Fig. 13, which is a turbine blade typical of modern engine designs.[12] A subcritical calculation using an extension to our mapping technique is presented in Fig. 14, which includes experimentally measured results. The downstream flow angle was specified for this computation, as the trailing edge is rounded. The agreement between our calculation and the experiment is good in part because the boundary layers apparently remained attached except near the trailing edge, so that viscous effects were small. This calculation was performed on a 16×65 grid and required 160 relaxation sweeps.

Conclusions

A stable, rapid, and accurate transonic flow calculation method has been generated using conformal mapping and relaxation techniques. An improved cascade to near-circle conformal transformation and a final mapping producing an improved grid system were introduced. The concept of "dynamic sweeping" was developed to stabilize the transonic relaxation process. Calculations are presented for known test cases to demonstrate the capability of these procedures.

Acknowledgment

The authors wish to acknowledge contributions to this project by M. Golecki.

References

[1]Garrick, I. E., "On the Plane Potential Flow Past a Lattice of Arbitrary Airfoils," NACA Rept. 688, 1944.

[2]Howell, A. R., "A Theory of Arbitrary Airfoils in Cascade," *The Philosophical Magazine*, Vol. 39, Dec. 1948, pp. 913-927.

[3]Legendre, R., "Work in Progress in France Related to Computation of Profiles for Turbomachine Blades by Hodograph Method," American Socity of Mechanical Engineers Paper 72-GT-41, March 1972.

[4]Frith, D. A., "Inviscid Flow through a Cascade of Thick, Cambered Airfoils, Part 1—Incompressible Flow," American Society of Mechanical Engineers Paper 73-GT-84, April 1973.

[5]Frith, D. A., "Inviscid Flow through a Cascade of Thick, Cambered Airfoils, Part 2—Compressible Flow," American Society of Mechanical Engineers, Paper 73-GT-85, April 1973.

[6]Jameson, A., "Iterative Solution of Transonic Flows Over Airfoils and Wings, Including Flows at Mach 1," *Communications on Pure and Applied Mathematics*, vol. XXVII, May 1974, pp. 283-309.

[7]Caughey, D. A. and Jameson, A., "Accelerated Iterative Calcultion of Transonic Nacelle Flowfields," AIAA Paper 76-100, Washington, D.C., 1976; submitted to *AIAA Journal*.

[8]Theodorsen, T. and Garrick, I. E., "General Potential Theory of Arbitrary Wing Sections," NACA TR 452, 1933.

[9]Ives, D. C., "A Modern Look at Conformal Mapping, Including Multiply Connected Regions," *AIAA Journal*, Vol. 14, Aug. 1976, pp. 1006-1011.

[10]Gostelow, J. P., "Potential Flow through Cascades—A Comparison Between Exact and Approximate Solutions," Aeronautical Research Council, London, CP 807, 1965.

[11]Korn, D. G., "Numerical Design of Transonic Cascades," Courant Inst. of Mathematical Sciences, ERDA Mathematics and Computing Lab., Rept. C00-3077-72, Jan. 1975.

[12]Langston, L. S., Nice, M. L., and Hooper, R. M., "Three-Dimensional Flow Within a Turbine Cascade Passage," American Society of Mechanical Engineers Paper 76-GT-50, March 1976.